

## Immunoassays

How to cite: *Angew. Chem. Int. Ed.* **2021**, *60*, 13042–13049

International Edition: doi.org/10.1002/anie.202103458

German Edition: doi.org/10.1002/ange.202103458

# Ratiometric Fluorescent Lateral Flow Immunoassay for Point-of-Care Testing of Acute Myocardial Infarction

Jing Wang<sup>†</sup>, Chenxing Jiang<sup>†</sup>, Jiening Jin, Liang Huang,\* Wenbo Yu, Bin Su,\* and Jun Hu\*

**Abstract:** We report the development of a highly sensitive ratiometric fluorescent lateral flow immunoassay (RFLFIA) strip for rapid and accurate detection of acute myocardial infarction biomarker, namely heart-type fatty acid binding protein (H-FABP). The RFLFIA strip works in terms of ratiometric change of fluorescence signal, arising from blending of fluorescence emitted by two composite nanostructures conjugated to capture and probe antibodies and inner filter effect of gold nanoparticles. In conjunction with using custom smartphone-based analytical device and tonality analysis, quantitative detection of H-FABP was achieved with a low limit of detection at  $0.21 \text{ ng mL}^{-1}$ . The RFLFIA strip can generate a visually distinguishable green-to-red color change around the threshold concentration of H-FABP ( $6.2 \text{ ng mL}^{-1}$ ), thus allowing the semi-quantitative diagnosis by the naked eye.

## Introduction

Acute myocardial infarction is the leading cause of sudden cardiac death. So its early and timely warning is highly important in the diagnosis and control of cardiovascular diseases.<sup>[1]</sup> Given the lack of specificity by signs and symptoms, the detection of myocardial biomarkers is considered to be a reliable method for acute myocardial infarction diagnosis.<sup>[2]</sup> For example, heart-type fatty acid binding protein (H-FABP), a biomarker of cardiac injury with a threshold value of  $6.2 \text{ ng mL}^{-1}$ , can be detected as early as 1.5 h after the first symptom.<sup>[3]</sup> However, the current clinic detection of H-FABP is usually based on either enzyme-linked immunosorbent assay or latex assay,<sup>[4]</sup> both of which are capable of providing reliable evaluation but require specific instruments, professional examiners and certain turnaround time, thus being

unsuitable for emergency case or self-testing by untrained patients at home. Because the prime time to treat an acute myocardial infarction is within 2 h,<sup>[5]</sup> there has been growing demand of developing an at-home blood test or point-of-care test (POCT) that allows the patients to rapidly and timely monitor H-FABP.

Lateral flow immunoassay (LFIA) is currently the state-of-art platform for POCT, thanks to its superiority of speediness, low-cost, portability and simplicity.<sup>[6]</sup> Among commercial LFIA, gold nanoparticles (AuNPs) and fluorescent microspheres are used predominantly as reporters to achieve optical signal readout.<sup>[7]</sup> AuNPs-based colorimetric LFIA is easy to use and can acquire results straightforwardly with the naked eye, which is however limited by the quantification ability and sensitivity.<sup>[8]</sup> In contrast, fluorescence-based LFIA (FLFIA) is advantageous in terms of sensitivity, because the optical signal can be amplified remarkably by doping microspheres with highly-luminescent molecular emitters or quantum dots (QDs).<sup>[9]</sup> Despite numerous FLFIAs have been developed and commercialized so far, some challenges still exist. First, similar to AuNPs-based LFIA, the naked eye visual inspection of FLFIA is also based on the change of color intensity (luminance), so that it is difficult to qualitatively or semi-quantitatively discriminate targets at a low concentration with a weakly colorful test-line, in particular for untrained examiners or patients.<sup>[10]</sup> Second, most reporters give rise to single-signal response, both accuracy and sensitivity of quantitative results are influenced by a number of analyte-independent parameters, such as reporter photobleaching, light scattering, excitation light fluctuation and so on.<sup>[11]</sup> Third, bulky instruments or devices are still needed to collect data, which are incompatible with on-site detection and unfriendly to resource-constrained end-users.<sup>[12]</sup> Therefore, solving these technical issues and promoting the widespread use of FLFIA are of continuously great interest.



Ratiometric fluorescence technology that relies on the intensity ratio of two or more emission bands has been widely used in the design of fluorescent sensors.<sup>[13]</sup> Unlike single fluorescence signal, the ratiometric scheme can minimize the external interference by self-calibration to improve the detection sensitivity.<sup>[14]</sup> Additionally, it can also output different colors with typical tonality (hue) to enhance the visual identification. Compared with color intensity, color hue is a superior strategy for naked eye readout, since hue is tunable and its variations are easy to differentiate.<sup>[15]</sup> Moreover, the hue changes along with the intensity variations of three primary colors (red-green-blue, RGB), hence the signal intensity ratio of different colors, such as R/G, can be utilized to quantify the target concentration with portable terminal

[\*] Dr. J. Wang,<sup>[†]</sup> C. Jiang,<sup>[†]</sup> J. Jin, Dr. L. Huang, Prof. J. Hu  
College of Chemical Engineering  
Zhejiang University of Technology, Hangzhou, 310014 (PR China)  
E-mail: lhuang@zjut.edu.cn  
hjzjut@zjut.edu.cn

Prof. B. Su  
Institute of Analytical Chemistry, Department of Chemistry  
Zhejiang University, Hangzhou, 310058 (PR China)  
E-mail: subin@zju.edu.cn

Dr. W. Yu  
College of Veterinary Medicine, China Agricultural University, Beijing  
Key Laboratory of Detection Technology for Animal Derived Food  
Safety, Beijing Laboratory for Food Quality and Safety  
Beijing, 100193 (PR China)

[†] These authors contributed equally to this work.

 Supporting information and the ORCID identification number(s) for the author(s) of this article can be found under:  
 <https://doi.org/10.1002/anie.202103458>.

devices (such as smartphone).<sup>[16]</sup> The universal design strategy for hue evolution is based on ratiometry with either a fixed reference signal or two reverse signal changes. By contrast, the latter presents a more sensitive intensity ratio change, and its sensitivity is on the same order of magnitude with the spectral analysis.<sup>[17]</sup> However, the utilization of double-signal-responsive strategy for the detection of protein biomarkers is still scarce, although it possesses a high sensitivity for visualization and is achievable via the energy transfer model.<sup>[18]</sup>

In this work we report a ratiometric fluorescence strategy for designing highly sensitive FLFIA (designated as RFLFIA) with hue signal readout. The RFLFIA strip enabled us to accomplish either naked eye readout of specific concentration of H-FABP or highly sensitive quantification of H-FABP with smartphone. As shown in Figure 1 (top panel), the fluorescent silica nanosphere loaded with AuNPs and red-light emitting CdSe/CdS/ZnS QDs (rQDs) (designated as SAQ) and tagged with anti-FABP 10E1 antibody (mAb1) is buried in the conjugate pad of test strip, meanwhile green-light emitting CdZnSe/CdS/ZnS QDs (gQDs) conjugated with anti-FABP 28 antibody (mAb2) (designated as mAb2-gQD) is immobilized in the test-line (T-line). In a positive assay, SAQ-mAb1 and mAb2-gQDs, together with H-FABP in the sample, form sandwich-like immunological complex structure at the T-line, resulting in the fluorescence color change from green to red. The change originates from the overlap of red fluorescence emitted by rQDs and green one by gQDs, as well as inner filter effect of AuNPs in SAQ on the green fluorescence, which is much more distinguishable than traditional FLFIA with only single fluorescence color change (bottom panel, Figure 1). Moreover, the color intensity ratio (R/G) of T-line also allows accurate quantitative analysis by combining with a custom strip analyzer and smartphone.

## Results and Discussion

SAQ and gQD are two core elements in RFLFIA. The former was prepared by loading AuNPs and rQDs into dendritic silica nanospheres (dSiO<sub>2</sub>) (see the Supporting Information and Scheme S1 therein for details). As shown in transmission electron microscopy (TEM) images (Figure 2a, b), dSiO<sub>2</sub> has a dendrimer-like structure with a diameter of ca. 275 nm. AuNPs and rQDs have an average diameter of ca. 11.0 nm and ca. 7.5 nm, respectively (Figure 2c, d). AuNPs were loaded to thiolated dSiO<sub>2</sub> via the formation of thiol-gold coordination.<sup>[19]</sup> The resulting dSiO<sub>2</sub>/AuNPs sphere consists of a number of AuNPs well distributed in the dendritic matrix (Figure 2e), which was then subjected to silanization and sol-gel reaction to fill the radial pores. Meanwhile, AuNPs were successfully buried inside the nanosphere (Figure 2f). After surface thiolation with (3-mercaptopropyl)trimethoxysilane again, rQDs can be subsequently assembled to the sphere, producing dSiO<sub>2</sub>/AuNPs/SiO<sub>2</sub>/rQDs (Figure 2g). Thus obtained sphere was eventually coated with another silica layer to prepare SAQ. TEM and high-angle annular dark-field scanning TEM (HAADF-STEM) images (Figure 2h, i), as well as elemental mapping by x-ray energy dispersive scattering (EDS; Figure 2j), confirm that AuNPs are uniformly distributed in the interior of SAQ sphere and rQDs are located only in the surface coating silica shell. Furthermore, the resulting SAQ displays a maximum absorption band at 533 nm and a fluorescence emission band at 626 nm (Supporting Information, Figure S1), indicating that SAQ retains the original plasmonic characteristic of AuNPs and fluorescent nature of rQDs. To conjugate with H-FABP antibody, namely mAb1, the surface of SAQ sphere was pre-derivatized with carboxylic groups (Supporting Information, Scheme S2).

To prepare gQDs, commercially available hydrophobic green-light emitting CdZnSe/CdS/ZnS QDs with an average

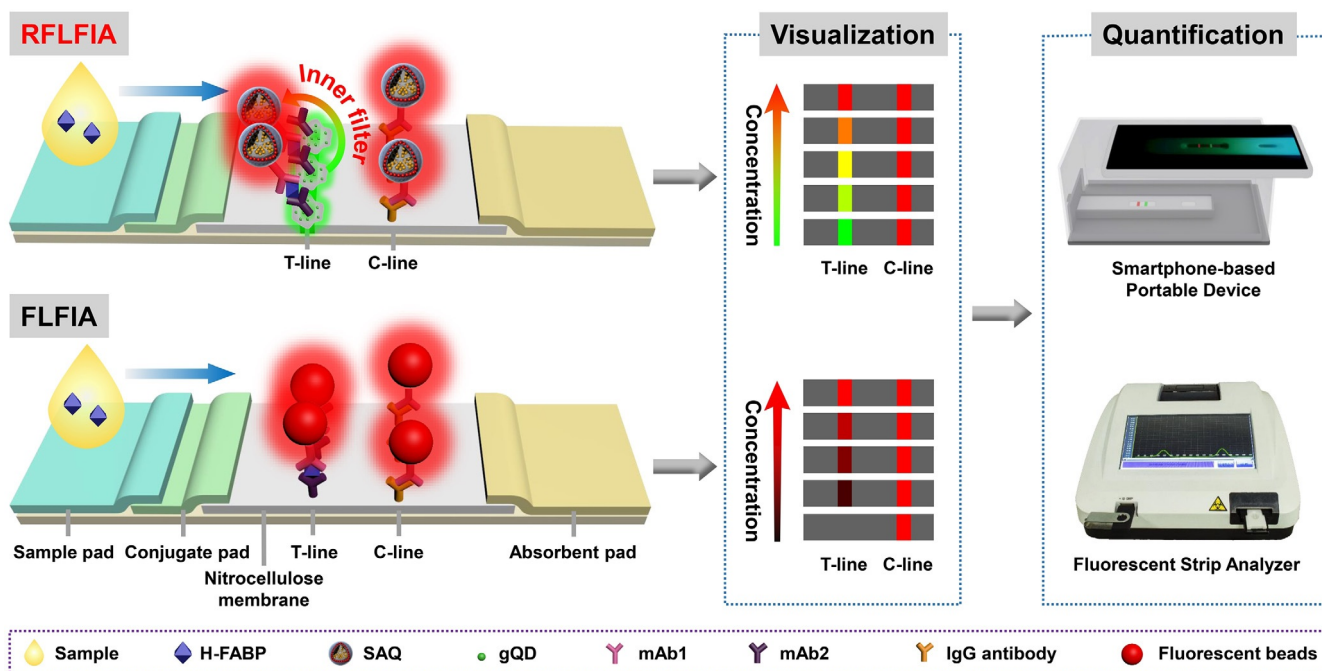


**Figure 1.** Illustration of RFLFIA and traditional FLFIA for visual and quantitative detection of H-FABP.



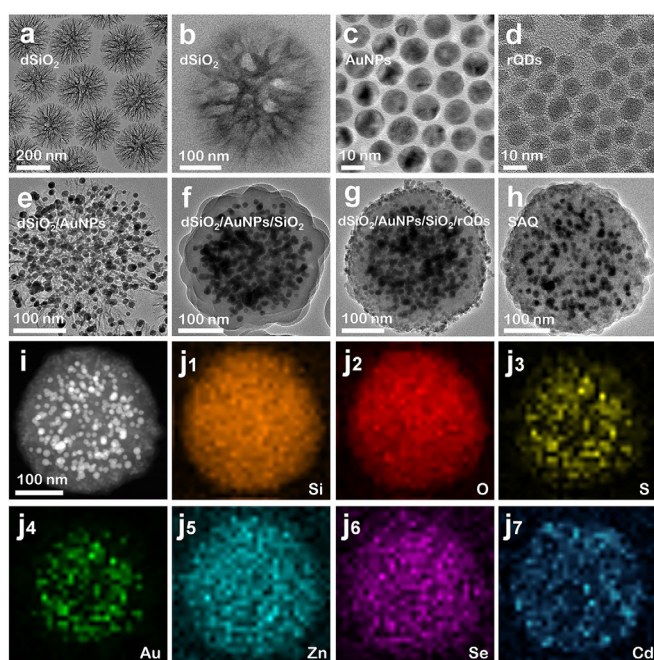


**Figure 2.** a)–h) TEM images of dSiO<sub>2</sub> (a), a single dSiO<sub>2</sub> (b), AuNPs (c), rQDs (d), dSiO<sub>2</sub>/AuNPs (e), dSiO<sub>2</sub>/AuNPs/SiO<sub>2</sub> (f), dSiO<sub>2</sub>/AuNPs/SiO<sub>2</sub>/rQDs (g) and SAQ (h). i) HAADF-STEM image of SAQ. j) EDS mapping of different elements (j<sub>1</sub>–j<sub>7</sub>) for a single SAQ nanosphere.

diameter of ca. 9.5 nm (Supporting Information, Figure S2a) were transferred from chloroform to water by surface encapsulation with amphiphilic poly(maleic anhydride-alt-1-octadecene) (Supporting Information, Scheme S3). The obtained carboxylated gQDs (Figure S2b) displayed a very slightly red-shifted fluorescence maximum at 524 nm with respect to the original one at 523 nm (Supporting Information, Figure S3).

Carboxylated SAQ and gQDs were then conjugated with H-FABP monoclonal antibodies (mAb1 and mAb2) by carbodiimide cross-linking reaction to form SAQ-mAb1 reporters and mAb2-gQDs capture probes. Note that the hydrodynamic sizes of both SAQ-mAb1 and mAb2-gQDs were increased after the antibody conjugation (Supporting Information, Figure S4), and their zeta potentials showed a reduced negative charge from  $-61.3$  to  $-20.7$  mV and from  $-52.0$  to  $-30.8$  mV (Supporting Information, Figure S5), respectively, indicating the successful antibody conjugation on the particle surface.<sup>[20]</sup> The conjugation was also confirmed by the fact that the obtained SAQ-mAb1 and mAb2-gQDs can specifically bind with FITC-labeled goat anti-mouse IgG (Supporting Information, Figure S6) and RBITC-labeled goat-anti-mouse IgG (Supporting Information, Figure S7), respectively.<sup>[21]</sup>

With RFLFIA, we intend to achieve two reverse fluorescent signal changes for H-FABP detection in a positive assay, which relies on the attenuation effect of AuNPs loaded to SAQ sphere on the fluorescence of gQDs, as well as ratiometric blending of fluorescence emitted by rQDs loaded to SAQ sphere and that by gQDs. To verify this hypothesis, the absorption, excitation and emission spectra of different nanostructures were compared. As shown in Figure 3 a, both

excitation (curve I) and emission (curve II) spectra of gQDs overlap well with the absorption spectra of AuNPs (curve III) and SAQ spheres (curve IV). This feature confirms the possibility of fluorescence attenuation by AuNPs or SAQ spheres via inner filter effect involving both excitation quenching (that is, competitive absorption) and radiative fluorescence quenching.<sup>[22]</sup> Indeed, as illustrated in Figure 3b, the fluorescence intensity of mAb2-gQD (black curve) decreased apparently in the presence of dSiO<sub>2</sub>/AuNPs/SiO<sub>2</sub>-mAb1 (red curve) or SAQ-mAb1 (blue curve).

Note that neither the fluorescence intensity of mAb2-gQD nor that of SAQ-mAb1 changed significantly after mixing with H-FABP antigens to form immunocomplex structure, namely SAQ-mAb1/antigen/mAb2-gQDs (green curve, Figure 3b). It implies that rQDs influence insignificantly the fluorescence of gQDs, although the emission spectrum of mAb2-gQDs also overlaps with the absorption spectrum of rQDs (Supporting Information, Figure S8). Given the closest approach and center-to-center distance between rQDs and gQDs in the immunocomplex structure are at least 28 nm and 162 nm, respectively, which are significantly larger than the Förster distance (ca. 9.4 nm), implying that non-radiative resonance energy transfer between two types of QDs is indeed unfavorable (see the Supporting Information, Figure S8 and its caption for details).

Above data corroborated a scheme involving ratiometric fluorescence change, which can be used for designing highly sensitive RFLFIA strip for H-FABP detection. As exemplified in Figure 1 (top panel, see also details in the Supporting Information), SAQ-mAb1 and mAb2-gQDs were loaded to and fixed in the conjugate pad and T-line of RFLFIA test strip, respectively. The control-line (C-line) was immobilized

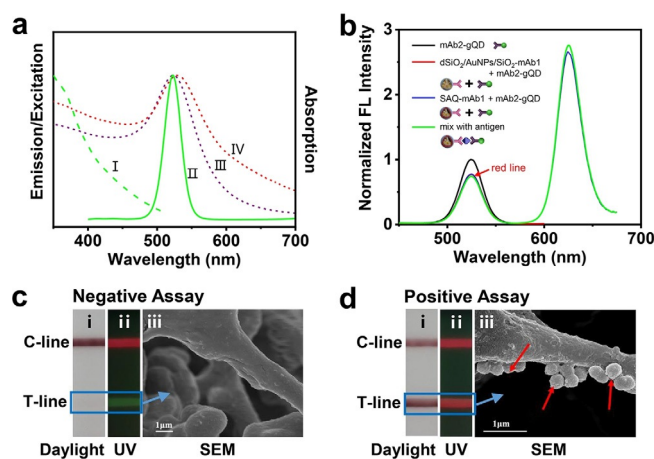


**Figure 3.** a) The excitation (curve I), emission (curve II) spectra of gQDs and the absorption spectra of AuNPs (curve III) and SAQ spheres (curve IV). b) The variation of emission of mAb2-gQDs (black curve) upon mixing with dSiO<sub>2</sub>/AuNPs/SiO<sub>2</sub>-mAb1 (red curve), SAQ-mAb1 (blue curve), both SAQ-mAb1 and H-FABP (green curve). The concentrations of mAb2-gQDs, dSiO<sub>2</sub>/AuNPs/SiO<sub>2</sub>-mAb1, SAQ-mAb1 and H-FABP are 1.4 nM, 20 μg mL<sup>-1</sup>, 20 μg mL<sup>-1</sup> and 1 μg mL<sup>-1</sup>, respectively. c, d) Photographs (i), fluorescence (ii) and SEM images (iii) of RFLFIA strip membrane after a negative (c) and positive assay (d, 50 ng mL<sup>-1</sup>). The red arrows annotate SAQ spheres captured in the T-line.

with goat-anti-mouse IgG antibodies. Upon adding sample solutions onto the sample pad, the lateral flow of liquid carries SAQ-mAb1 to migrate toward the absorbent pad via the capillary effect. For a negative assay where H-FABP was absent, the T-line was colorless under daylight (Figure 3c, i) and remained green under UV illumination (Figure 3c, ii). In this case, no immunocomplex was formed and thus no SAQ spheres were found in the T-line (Figure 3c, iii). In contrast, in the case of a positive test, SAQ-mAb1 was captured in the T-line by forming SAQ-mAb1/H-FABP/mAb2-gQDs complex (Figure 3d, iii). Therefore, the T-line appeared maroon under daylight (Figure 3d, i) whereas turned red under UV (Figure 3d, ii).

At present FLFIA result readout usually relies on dynamic scanning and acquisition of light intensity by complicated optical system,<sup>[23]</sup> which heavily limits its practical applications in POCT. In addition, the existing reader can only recognize one signal of a certain wavelength range at a time, which is also incompatible with RFLFIA developed herein. To solve these issues, we fabricated a portable reading device that consists of a smartphone, 3D-printed top and bottom covers, strip holder, light emitting diode (LED), polymer lithium ion battery and two optical filters (as shown in Figure 4a; Supporting Information, Figure S9a). The miniaturized device had only an overall dimension of ca. 140 mm × 75 mm × 55 mm. The LED functioned as the light source, the light from which was filtered by 365 nm band-pass filter and then illuminated the detection zone of RFLFIA strip at an incidence angle of 45°. The generated fluorescence signals passed a 500 nm long-pass filter to reduce background noise and were then captured by the CMOS image sensor of smartphone.

The top panel of Figure 4b displays the images of detection zones of RFLFIA strips captured by the custom device. 75  $\mu\text{L}$  of sample solutions containing different concentrations of H-FABP (from 0 to 50  $\text{ng mL}^{-1}$ ) were added onto the sample pad. And the reaction time was set to 10 min (as optimized in the Supporting Information, Figure S10). Clearly, with the increase of H-FABP concentration, the T-line of RFLFIA appeared a distinguishable fluorescence color change from green to red. It should be noticed that the fluorescence color of T-line displayed a sensitive color change from yellow to orange when the concentrations of H-FABP was increased from 3.12 to 6.25  $\text{ng mL}^{-1}$ . This color change is beneficial to rapid test because a concentration higher than 6.2  $\text{ng mL}^{-1}$  indicates cardiac injury suffered.

To gain more accurate information from fluorescence images, we used an app called "Color Picker" to extract hue and RGB values (Supporting Information, Figure S9b, c). The former can be derived using the HSL model, which describes colors in terms of hue (H), saturation (S) and lightness (L).<sup>[24]</sup> The whole hue is represented by a 360° color wheel with an angle from 0° to 360°. Red, green, and blue colors correspond to the angles of 0°, 120° and 240°, respectively, in the wheel. For example, when the color changes from green to red, the hue value turns from 120° to 0°. As shown in Figure 4c, the hue value at a concentration of 6.2  $\text{ng mL}^{-1}$  is about 20. It means that, when the concentration of H-FABP is higher than 6.2  $\text{ng mL}^{-1}$ , the hue value is less

than 20. Therefore, the hue-based image analysis can enhance the accuracy of test results by directly recognizing the fluorescence color rather than measuring the fluorescence intensity.

For the sake of more quantitative analysis, RGB values can be also extracted from the deconvolution of each image into three primary color codes, namely red, green, and blue. And each color can be further divided into 256 integer values in terms of its brightness.<sup>[25]</sup> As displayed in Figure 4d, with the increase of H-FABP concentration, the green fluorescence intensity and G value declined, whereas the red one and R value increased, resulting in a double-signal reverse fluorescence change. A control experiment using a 525 nm bandpass filter in the front of smartphone detector also confirmed the continuous decrease of green fluorescence, as shown in the Supporting Information, Figure S11. The ratio between red and green channel (R/G value) exhibited a linear relationship with the concentration of H-FABP in the range of 0–6.25  $\text{ng mL}^{-1}$  (Figure 4e). The limit of detection (LOD) was calculated to be 0.21  $\text{ng mL}^{-1}$  ( $3\sigma/m$ , in which  $\sigma$  is the standard deviation of the blank and  $m$  the slope of the linear dynamic range).<sup>[26]</sup> In comparison with the lab-instrument based strategies previously reported for H-FABP detection (Supporting Information, Table S1), the RFLFIA strip test yielded rapid and sensitive quantitative results in a more convenient manner. Meanwhile, in comparison with conventional POCT approaches that only tell yes/no, the current RFLFIA strip test can provide a more accurate semiquantitative and even quantitative answer.

To further verify the superiority of RFLFIA, traditional FLFIA with single-signal response (as illustrated in Figure 1, bottom) was also prepared for comparison, in which the T-line was immobilized with only mAb2 instead of mAb2-gQDs. As can be seen in Figure 4b (bottom), only red fluorescence was captured at the T-line at a high enough concentration of H-FABP, which was generated by rQDs in SAQ. It was hard to read out the variation of H-FABP concentration according to the color change. Although the change of hue value caused by weak green fluorescence background (most likely originated from BSA used for pretreating conjugate pad) was also observed (Figure 4f), the resulting color change of T-line was insensitive to the naked eye. Moreover, the R value can be also fitted for quantitative analysis (Figure 4g), but the LOD was calculated to be 0.59  $\text{ng mL}^{-1}$  (Figure 4h), ca. 3 times higher than that of RFLFIA.

In a control experiment,  $\text{SiO}_2/\text{rQDs}/\text{SiO}_2$  nanospheres with size similar to SAQ ones (Supporting Information, Figures S12 and S13) were also synthesized to replace SAQ to prepare  $\text{SiO}_2/\text{rQDs}/\text{SiO}_2$  based RFLFIA (designated as RFLFIA-2). Although similar results were obtained, the fluorescent color change was more sluggish (Supporting Information, Figures S14 and S15a). Moreover, as can be seen from the Supporting Information, Figure S15b, the G value of RFLFIA-2 changed insignificantly and therefore the R/G ratio changed more slowly too. The results prove the essential role of inner filter effect of AuNPs in achieving highly sensitive visual and quantitative ratiometric fluorescence change.

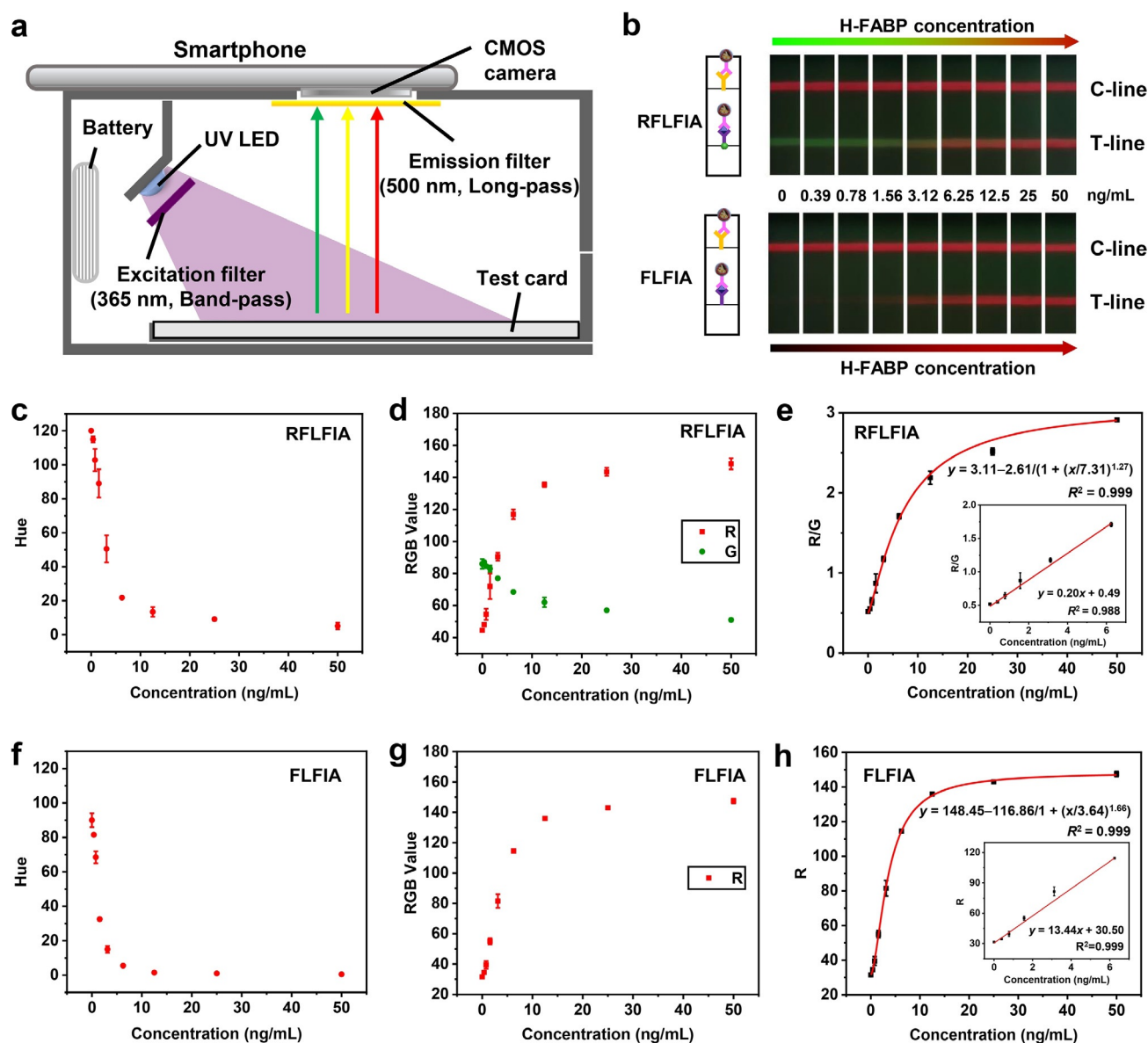


**Figure 4.** a) Illustration of smartphone-based portable fluorescence reading device. b) Fluorescence images of RFLFIA and conventional FLFIA strips at different concentrations of H-FABP (from 0 to 50 ng mL<sup>-1</sup>). c,d) The dependence of hue (c), R and G (d) values of the T-line of RFLFIA strips on the concentration of H-FABP. e) The relationship of R/G ratio of the T-line of RFLFIA strips with H-FABP concentration. Inset shows the concentration dependence of R/G ratio in the low concentration range. f,g) The dependence of hue (f) and R (g) values of the T-line of conventional FLFIA strips on the concentration of H-FABP. h) The relationships of R value of the T-line of conventional FLFIA strips with H-FABP concentration. Inset: the linear dependence of R value in the low concentration range.

To evaluate the specificity of RFLFIA for H-FABP recognition, several general cardiac markers and proteins in human blood, such as cardiac troponin I (cTnI), N-terminal pro brain natriuretic peptide (NT-proBNP), myoglobin (Myo), human serum albumin (HSA) and C-reactive protein (CRP), were selected as negative controls. The photographs under daylight and fluorescence images under UV illumination were both recorded. As compared in Figure 5 a and b, the presence of H-FABP made the T-line appear maroon under daylight, while it turned from green to orange under UV illumination. In contrast, there were no obvious color changes for all controlled samples. Moreover, the R/G value obtained with H-FABP was much larger than other negative controls

and blank control (Figure 5c), even if the concentration of controls was 1000-fold higher than that of H-FABP. These data prove the high specificity of RFLFIA.

We also implemented the real sample analysis using RFLFIA strips. The recoveries and coefficients of variation (CV) for the analysis of five H-FABP-spiked fetal bovine serum samples at five different target concentrations, namely 3.12, 6.25, 12.5, 25, and 50 ng mL<sup>-1</sup>. The test procedure was exhibited in the Supporting Information, Video S1. As shown in Table 1, the average recovery value fell in a range of 97.95–109.50% and CV was < 10.36%, suggesting an acceptable accuracy and precision for quantitative H-FABP detection. Furthermore, the RFLFIA test strips could be stored for



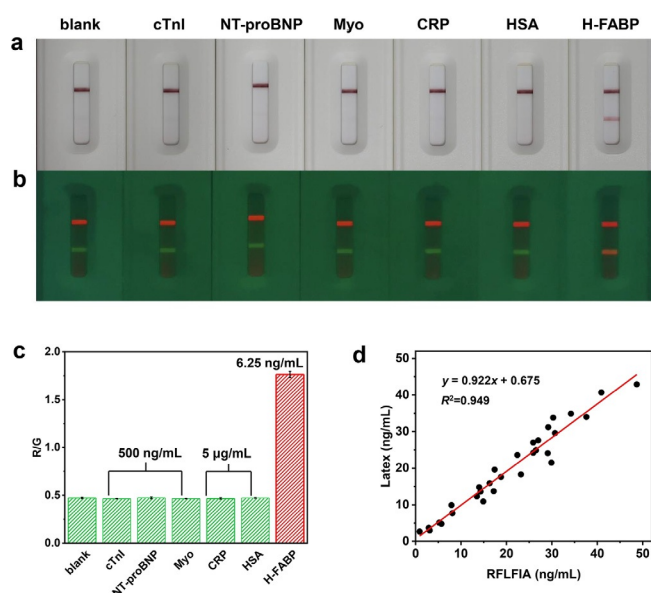


**Figure 5.** a)–c) Photographs (a), fluorescence images (b) and corresponding histogram (c) for the specificity of RFLFIA test strips toward H-FABP detection. d) Correlation analysis of the detection results between RFLFIA and clinically latex agglutination test of 30 human serum samples with the concentration of H-FABP from 2.5 to 42.9 ng mL<sup>-1</sup>.

**Table 1:** Recoveries and coefficients of variation (CV) for the detection of H-FABP in fetal bovine serum ( $n=5$ ) using RFLFIA strips.

Analyte	Added [ng mL <sup>-1</sup> ]	Detected [ng mL <sup>-1</sup> ]	Recovery [%]	CV [%]
H-FABP	3.12	3.28 ± 0.13	105.11	3.93
	6.25	6.84 ± 0.31	109.50	4.57
	12.5	12.59 ± 1.30	100.72	10.36
	25	24.49 ± 1.86	97.95	7.58
	50	54.42 ± 4.32	108.85	7.94

28 days at room temperature (Supporting Information, Figure S16), displaying a good stability for wide applications in low-resource settings.

Encouraged by the excellent performance shown above, the RFLFIA strip was applied to clinical detection of H-FABP in real serum samples. The correlation between results obtained with RFLFIA strips and clinical latex agglutination tests for 30 samples was analyzed. As shown in Figure 5 d, in the concentration range from 2.5 to 42.9 ng mL<sup>-1</sup>, a good linear correlation of two methods was obtained with a correlation coefficient ( $R^2$ ) of 0.949, indicating the high reliability of RFLFIA for POC diagnosis of clinical samples.

On the other hand, as shown in Figure 4b, with the increase of H-FABP concentration, the T-line of RFLFIA generated an apparent distinguishable green-to-red color change in the concentration range of 0–12.5 ng mL<sup>-1</sup>. Considering that the threshold value for clinic diagnosis of myocardial injury, namely 6.2 ng mL<sup>-1</sup>, falls within this range, the result in Figure 4b implies the possibility of estimating semi-quantitatively the specific H-FABP concentration and achieving diagnostic purpose by the naked-eye readout. To examine the practicability and reliability, semi-quantitative

naked-eye readout tests were performed with independent users. As displayed in Figure 6, with the increase of H-FABP concentration from 0 to 8 ng mL<sup>-1</sup>, the T-line of RFLFIA illustrated a visually recognizable green-to-orange red color change (Figure 6a, top panel), with which a color reference chart can be generated (Figure 6a, bottom panel). Subsequently, naked-eye signal readout by 11 independent users was implemented (see the Supporting Information and Figure S17 therein for details). Six samples containing different concentrations of H-FABP (0, 1, 2, 4, 6.2, and 8 ng mL<sup>-1</sup>) were analyzed for 3 times using RFLFIA strips, and the images of T-lines were interpreted with the naked eye by 11 independent users according to the color reference chart (totally  $3 \times 11 = 33$  readouts for each sample). All readouts made by users are summarized and compared in Figure 6b. The accuracy of determining a specific concentration was calculated to be 72.7–97.0%, indicating that RFLFIA strips indeed enable reproducible and reliable visual detection of H-FABP as

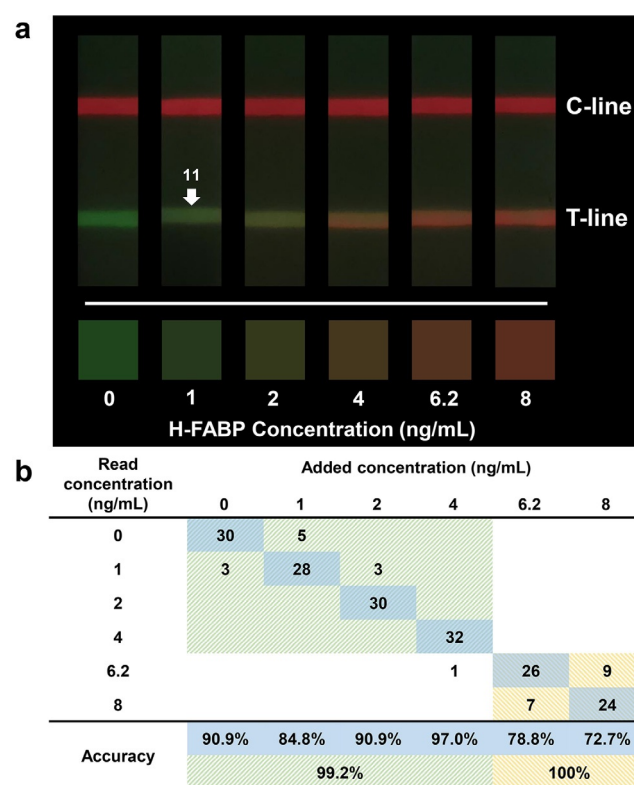


**Figure 6.** a) Fluorescence photographs of T-line and C-line of RFLFIA strips at 6 different concentrations of H-FABP. The images of T-line were used for generating the color reference chart (bottom). The white arrow and number indicate the test strips identifying the visible LOD interpreted by 11 independent users. b) Semi-quantitative naked-eye readout results for the analysis of 6 samples containing different concentrations of H-FABP for 3 times by 11 independent users ( $3 \times 11 = 33$  readouts for each sample, and totally  $3 \times 11 \times 6 = 198$  readouts for all). Numerals represent the times for each sample image interpreted by independent users. Accuracy is defined as the proportion of correct readouts among 33 readouts. Note that the images were placed in a fully random order before naked-eye readout (see the Supporting Information, Figure S17 for details). In all cases, we used HUAWEI P30 smartphone to capture images with an irradiation of 365 nm light and 500 nm long-pass filter.

simple as reading a pH test strip. The visual LOD interpreted by multiple users was ca.  $1 \text{ ng mL}^{-1}$ .<sup>[10]</sup> Moreover, if counting the detection of H-FABP at a concentration below and above the threshold value ( $6.2 \text{ ng mL}^{-1}$ ), the overall accuracy is 99.2% and 100%, respectively, verifying the feasibility of diagnosing cardiac injury suffered by the naked eye.

## Conclusion

We have developed a brand-new RFLFIA platform for quantitative and visual detection of H-FABP by using SAQ as reporters and gQDs as capture probes, respectively. The results confirm the sensing mechanism that target-induced inner filter effect between the SAQ and gQDs leads to an increase of red emission along with a decrease of green emission accompanied by a clear discernible color transition from green to red. By combining with a low-cost and straightforward intelligent analytical device composed of a 3D-printed compact attachment and smartphone, a LOD as low as  $0.21 \text{ ng mL}^{-1}$  is obtained, which is more accurate and sensitive than traditional FLFIA with only single signal response. This priority enables highly sensitive quantitative analysis of H-FABP in clinical serum samples. Moreover, RFLFIA strip also allows a sensitive naked-eye semi-quantitative readout of the specific H-FABP concentration through color change as simple as reading a pH test strip, with a visual LOD of ca.  $1 \text{ ng mL}^{-1}$ . The sensitivity is appealing and promising for on-site analysis and self-testing. We believe this strategy can be used for developing LFIA for rapid and accurate point-of-care diagnosis.

## Acknowledgements

The authors acknowledge the financial support from the National Natural Science Foundation of China (21875218, U1909214, 51672248, and 51872261), the Zhejiang Provincial Natural Science Foundation (LY21B050001, LGF20B010001, and LR19E020002).

## Conflict of interest

The authors declare no conflict of interest.

**Keywords:** H-FABP · immunoassays · point-of-care · ratiometric fluorescence · visual detection

- [1] a) J. P. Bassand, C. W. Hamm, D. Ardissino, E. Boersma, A. Budaj, F. Fernandez-Aviles, K. A. A. Fox, D. Hasdai, E. M. Ohman, L. Wallentin, W. Wijns, A. Vahanian, J. Camm, R. De Caterina, V. Dean, K. Dickstein, G. Filippatos, S. D. Kristensen, P. Widimsky, K. McGregor, U. Sechtem, M. Tendera, I. Hellemans, J. L. Z. Gomez, S. Silber, C. Funck-Brentano, S. D. Kristensen, F. Andreotti, W. Benzer, M. Bertrand, A. Betriu, R. De Caterina, J. DeSutter, V. Falk, A. F. Ortiz, A. Gitt, Y. Hasin, K. Huber, R. Kornowski, J. Lopez-Sendon, J. Morais, J. E. Nordrehaug, S. Silber, P. G. Steg, K. Thygesen, M. Tubaro,

- A. G. G. Turpie, F. Verheugt, S. Windecker, *Eur. Heart J.* **2007**, *28*, 1598–1660; b) J. L. Anderson, C. D. Adams, E. M. Antman, C. R. Bridges, R. M. Califf, D. E. Casey, Jr., W. E. Chavey II, F. M. Fesmire, J. S. Hochman, T. N. Levin, A. M. Lincoff, E. D. Peterson, P. Theroux, N. K. Wenger, R. S. Wright, H. Jneid, S. M. Ettinger, T. G. Ganiats, A. M. Lincoff, G. J. Philippides, J. P. Zidar, et al., *Circulation* **2013**, *127*, e663–828; c) K. Thygesen, J. S. Alpert, A. S. Jaffe, M. L. Simoons, B. R. Chaitman, H. D. White, et al., *J. Am. Coll. Cardiol.* **2012**, *60*, 1581–1598.
- [2] a) D. A. Morrow, C. P. Cannon, R. L. Jesse, L. K. Newby, J. Ravkilde, A. B. Storror, A. H. Wu, R. H. Christenson, et al., *Circulation* **2007**, *115*, e356–375; b) M. Roffi, C. Patrono, J. P. Collet, C. Mueller, M. Valgimigli, F. Andreotti, J. J. Bax, M. A. Borger, C. Brotons, D. P. Chew, B. Gencer, G. Hasenfuss, K. Kjeldsen, P. Lancellotti, U. Landmesser, J. Mehilli, D. Mukherjee, R. F. Storey, S. Windecker, E. S. C. S. D. Group, *Eur. Heart J.* **2016**, *37*, 267–315.
- [3] a) C. J. McCann, B. M. Glover, I. B. A. Menown, M. J. Moore, J. McEneny, C. G. Owens, B. Smith, P. C. Sharpe, I. S. Young, J. A. Adgey, *Eur. Heart J.* **2008**, *29*, 2843–2850; b) O. Fumio, S. Koichi, O. Yasuhiko, K. Keishiro, A. Kumiko, K. Hiroshi, N. Shinzo, I. Hiroo, S. Noriyuki, T. Takao, *Clin. Chem. Lab. Med.* **2000**, *38*, 231–238.
- [4] a) K. W. H. Wodzig, M. M. A. L. Pelsers, G. J. van der Vusse, W. Roos, J. F. C. Glatz, *Ann. Clin. Biochem.* **1997**, *34*, 263–268; b) M. Robers, F. F. Van der Hulst, M. A. J. G. Fischer, W. Roos, C. E. Salud, H.-G. Eisenwiener, J. F. C. Glatz, *Clin. Chem.* **1998**, *44*, 1564–1567.
- [5] B. R. Brodie, C. Hansen, T. D. Stuckey, S. Richter, D. S. VerSteeg, N. Gupta, W. E. Downey, M. Pulsipher, *J. Am. Coll. Cardiol.* **2006**, *47*, 289–295.
- [6] a) J. S. Gootenberg, O. O. Abudayyeh, M. J. Kellner, J. Joung, J. J. Collins, F. Zhang, *Science* **2018**, *360*, 439–444; b) G. Sciutto, M. Zangheri, L. Anfossi, M. Guardigli, S. Prati, M. Mirasoli, F. Di Nardo, C. Baggiani, R. Mazzeo, A. Roda, *Angew. Chem. Int. Ed.* **2018**, *57*, 7385–7389; *Angew. Chem.* **2018**, *130*, 7507–7511; c) V. Tran, B. Walkenfort, M. Konig, M. Salehi, S. Schlucker, *Angew. Chem. Int. Ed.* **2019**, *58*, 442–446; *Angew. Chem.* **2019**, *131*, 450–455; d) H. de Puig, I. Bosch, L. Gehrke, K. Hamad-Schifferli, *Trends Biotechnol.* **2017**, *35*, 1169–1180; e) J. H. Soh, H.-M. Chan, J. Y. Ying, *Nano Today* **2020**, *30*, 100831; f) E. Costa, E. Climent, S. Ast, M. G. Weller, J. Canning, K. Rurack, *Analyst* **2020**, *145*, 3490–3494; g) E. Climent, M. Biyikal, D. Gröninger, M. G. Weller, R. Martínez-Máñez, K. Rurack, *Angew. Chem. Int. Ed.* **2020**, *59*, 23862–23869; *Angew. Chem.* **2020**, *132*, 24071–24078.
- [7] a) L. Sorell, J. A. Garrote, B. Acevedo, E. Arranz, *Lancet* **2002**, *359*, 945–946; b) L. Guo, X. Wu, L. Liu, H. Kuang, C. Xu, *Small* **2018**, *14*, 1701782; c) X. Huang, Y. Zhou, L. Ding, G. Yu, Y. Leng, W. Lai, Y. Xiong, X. Chen, *Small* **2019**, *15*, 1903861; d) J. Hu, Y. Z. Jiang, L. L. Wu, Z. Wu, Y. Bi, G. Wong, X. Qiu, J. Chen, D. W. Pang, Z. L. Zhang, *Anal. Chem.* **2017**, *89*, 13105–13111.
- [8] Y. Zhou, L. Ding, Y. Wu, X. Huang, W. Lai, Y. Xiong, *TrAC Trends Anal. Chem.* **2019**, *112*, 147–160.
- [9] a) L. Huang, T. Liao, J. Wang, L. Ao, W. Su, J. Hu, *Adv. Funct. Mater.* **2018**, *28*, 1705380; b) X. Huang, Z. P. Aguilar, H. Li, W. Lai, H. Wei, H. Xu, Y. Xiong, *Anal. Chem.* **2013**, *85*, 5120–5128; c) H. Duan, X. Huang, Y. Shao, L. Zheng, L. Guo, Y. Xiong, *Anal. Chem.* **2017**, *89*, 7062–7068; d) J. Hu, Z. L. Zhang, C. Y. Wen, M. Tang, L. L. Wu, C. Liu, L. Zhu, D. W. Pang, *Anal. Chem.* **2016**, *88*, 6577–6584; e) Z. Qie, Q. Liu, W. Yan, Z. Gao, W. Meng, R. Xiao, S. Wang, *Anal. Chem.* **2019**, *91*, 9530–9537; f) C. Wang, X. Yang, B. Gu, H. Liu, Z. Zhou, L. Shi, X. Cheng, S. Wang, *Anal. Chem.* **2020**, *92*, 15542–15549; g) Y. Yao, W. Guo, J. Zhang, Y. Wu, W. Fu, T. Liu, X. Wu, H. Wang, X. Gong, X. J.

- Liang, J. Chang, *ACS Appl. Mater. Interfaces* **2016**, *8*, 22963–22970.
- [10] K. Misawa, T. Yamamoto, Y. Hiruta, H. Yamazaki, D. Citterio, *ACS Sens.* **2020**, *5*, 2076–2085.
- [11] a) G. Zhu, X. Yin, D. Jin, B. Zhang, Y. Gu, Y. An, *TrAC Trends Anal. Chem.* **2019**, *111*, 100–117; b) Z. Luo, T. Lv, K. Zhu, Y. Li, L. Wang, J. J. Gooding, G. Liu, B. Liu, *Angew. Chem. Int. Ed.* **2020**, *59*, 3131–3136; *Angew. Chem.* **2020**, *132*, 3155–3160.
- [12] a) M. Zarei, *TrAC Trends Anal. Chem.* **2017**, *91*, 26–41; b) X. Ding, M. G. Mauk, K. Yin, K. Kadimisetty, C. Liu, *Anal. Chem.* **2019**, *91*, 655–672.
- [13] a) K. Zhang, H. Zhou, Q. Mei, S. Wang, G. Guan, R. Liu, J. Zhang, Z. Zhang, *J. Am. Chem. Soc.* **2011**, *133*, 8424–8427; b) D. Cheng, Y. Pan, L. Wang, Z. Zeng, L. Yuan, X. Zhang, Y.-T. Chang, *J. Am. Chem. Soc.* **2017**, *139*, 285–292; c) R. Jia, W. Tian, H. Bai, J. Zhang, S. Wang, J. Zhang, *Nat. Commun.* **2019**, *10*, 795; d) A. Zhu, Q. Qu, X. Shao, B. Kong, Y. Tian, *Angew. Chem. Int. Ed.* **2012**, *51*, 7185–7189; *Angew. Chem.* **2012**, *124*, 7297–7301; e) Z. Liu, X. Zhou, Y. Miao, Y. Hu, N. Kwon, X. Wu, J. Yoon, *Angew. Chem. Int. Ed.* **2017**, *56*, 5812–5816; *Angew. Chem.* **2017**, *129*, 5906–5910.
- [14] a) X. Huang, J. Song, B. C. Yung, X. Huang, Y. Xiong, X. Chen, *Chem. Soc. Rev.* **2018**, *47*, 2873–2920; b) M. H. Lee, J. S. Kim, J. L. Sessler, *Chem. Soc. Rev.* **2015**, *44*, 4185–4191; c) Y. Cui, R. Song, J. Yu, M. Liu, Z. Wang, C. Wu, Y. Yang, Z. Wang, B. Chen, G. Qian, *Adv. Mater.* **2015**, *27*, 1420–1425.
- [15] C. Jiang, B. Liu, M.-Y. Han, Z. Zhang, *Small Methods* **2018**, *2*, 1700379.
- [16] a) E. Petryayeva, W. R. Algar, *Anal. Chem.* **2014**, *86*, 3195–3202; b) K. G. Shah, V. Singh, P. C. Kauffman, K. Abe, P. Yager, *Anal. Chem.* **2018**, *90*, 6967–6974; c) S. Chu, H. Wang, X. Ling, S. Yu, L. Yang, C. Jiang, *ACS Appl. Mater. Interfaces* **2020**, *12*, 12962–12971.
- [17] R. Gui, H. Jin, X. Bu, Y. Fu, Z. Wang, Q. Liu, *Coord. Chem. Rev.* **2019**, *383*, 82–103.
- [18] a) E. Petryayeva, W. R. Algar, *Anal. Chem.* **2013**, *85*, 8817–8825; b) M. O. Noor, U. J. Krull, *Anal. Chem.* **2014**, *86*, 10331–10339; c) E. Petryayeva, W. R. Algar, *Analyst* **2015**, *140*, 4037–4045; d) Y.-Q. Yang, Y.-C. Yang, M.-H. Liu, Y.-H. Chan, *Anal. Chem.* **2020**, *92*, 1493–1501.
- [19] V. L. Colvin, A. N. Goldstein, A. P. Alivisatos, *J. Am. Chem. Soc.* **1992**, *114*, 5221–5230.
- [20] a) C.-W. Yen, H. de Puig, J. O. Tam, J. Gómez-Márquez, I. Bosch, K. Hamad-Schifferli, L. Gehrke, *Lab Chip* **2015**, *15*, 1638–1641; b) H. Xu, Z. P. Aguilar, L. Yang, M. Kuang, H. Duan, Y. Xiong, H. Wei, A. Wang, *Biomaterials* **2011**, *32*, 9758–9765.
- [21] C.-Y. Wen, L.-L. Wu, Z.-L. Zhang, Y.-L. Liu, S.-Z. Wei, J. Hu, M. Tang, E.-Z. Sun, Y.-P. Gong, J. Yu, D.-W. Pang, *ACS Nano* **2014**, *8*, 941–949.
- [22] J. Zhang, R. Zhou, D. Tang, X. Hou, P. Wu, *TrAC Trends Anal. Chem.* **2019**, *110*, 183–190.
- [23] R. C. Wong, H. Y. Tse, *Lateral Flow Immunoassay*, Humana Press, New York, **2009**.
- [24] K. Cantrell, M. M. Erenas, I. de Orbe-Payá, L. F. Capitán-Vallvey, *Anal. Chem.* **2010**, *82*, 531–542.
- [25] D. Quesada-González, A. Merkoçi, *Biosens. Bioelectron.* **2017**, *92*, 549–562.
- [26] C. C. Fang, C. C. Chou, Y. Q. Yang, T. Wei-Kai, Y. T. Wang, Y. H. Chan, *Anal. Chem.* **2018**, *90*, 2134–2140.

Manuscript received: March 10, 2021

Accepted manuscript online: April 1, 2021

Version of record online: May 5, 2021